Optics Letters

Dynamic structured illumination for confocal microscopy

Guillaume Nœtinger, Fabrice Lemoult, and Sébastien M. Popoff*

Institut Langevin, ESPCI Paris, Université PSL, CNRS, Paris 75005, France
**sebastien.popoff@espci.fr*

Received 6 September 2023; revised 10 November 2023; accepted 16 January 2024; posted 25 January 2024; published 22 February 2024

Structured illumination enables the tailoring of an imaging device's optical transfer function to enhance resolution. We propose the incorporation of a temporal periodic modulation, specifically a rotating mask, to encode multiple transfer functions in the temporal domain. This approach is demonstrated using a confocal microscope configuration. At each scanning position, a temporal periodic signal is recorded. By filtering around each harmonic of the rotation frequency, multiple images of the same object can be constructed. The image carried by the *n*th harmonic is a convolution of the object with a phase vortex of topological charge *n*, similar to the outcome when using a vortex phase plate as an illumination. This enables the collection of chosen high spatial frequencies from the sample, thereby enhancing the spatial resolution of the confocal microscope.

https://doi.org/10.1364/OL.500524

The optical confocal microscope [1], an imaging device extensively utilized for decades, has proven invaluable for scientists investigating phenomena at the scale of hundreds of nanometers. These researchers, including biologists and material scientists, benefit from the device's ability to filter out-of-focus light. This is known as *optical sectioning*. This feature enables the capture of high contrast images even in diffusive samples such as a biological tissue [2]. The high-resolution capabilities of the confocal microscope are particularly beneficial for fluorescent imaging [3]. Combined with a depletion beam in the STED configuration, the device can achieve superresolution, yielding precise structural insights at the cellular level [4]. However, fluorescent markers present limitations, including their potential toxicity and the prerequisite treatment of the sample, making them unsuitable in some contexts. Consequently, the development of optical label-free superresolution microscopy would be highly advantageous in numerous practical applications [5,6].

Broadly, the inclusion of time in an optical scheme opens new possibilities [7]. Mechanical scanning as used in STED, illumination and acquisition sequences as seen in STORM [8], and structured illumination [9], as well as the analysis of emission fluctuations in SOFI [10], all exemplify the prevalent use of time as an additional degree of freedom in numerous superresolution techniques. For example, recent work involving illumination modulation in a fluorescent sample with time-varying structured illumination has demonstrated a remarkable precision in localization [11].

In this article, we address the challenge of label-free superresolution in the far-field utilizing an analogous approach that capitalizes on the temporal domain to enhance the volume of data gathered from the object for image reconstruction. To that end, we suggest incorporating wavefront shaping techniques into a standard confocal microscope to introduce a temporal modulation in the signal acquired at each scanning point. The resultant additional degrees of freedom could enhance the space-bandwidth product [12] of the confocal microscope, leading to an improved resolution.

Concept. In the absence of fluorescent probes, the confocal microscope demonstrates a modest improvement in lateral resolution compared to the full-field configuration. In a full-field microscope, the coherent point-spread function (PSF) corresponds to the 2D Fourier transform of the pupil function. With a circular pupil, it is recognized as the Airy function. Owing to the scanning process and under the approximation of a point-like detector, the coherent PSF of the confocal microscope can be expressed as the product of the illumination and collection of PSFs [13]. In a symmetric configuration, its width is smaller than that of the full-field microscope. Using a Gaussian approximation of the PSF, the improvement in the lateral resolution is estimated to be on the order of $\sqrt{2}$ which is about 40%.

In terms of spatial frequencies, the coherent transfer function (CTF) of a full-field microscope is dictated by the shape of the microscope objective's pupil. For a circular pupil, the CTF takes the form of a circular step function: spatial frequencies with a modulus greater than NA/λ are filtered out, where NA represents the numerical aperture and λ is the wavelength. All spatial frequencies within this zone are transmitted with the same amplitude. In the confocal microscope, the CTF is the convolution of the illumination and collection of CTFs [14]. Assuming a symmetric configuration for the illumination and collection, the confocal microscope possesses a well-known conical CTF of support twice as large as the full-field CTF [13]. This means that the highest transmitted spatial frequency, $2NA/\lambda$, is twice that in the full-field configuration. However, the gain diminishes linearly, peaking at low spatial frequencies and reaching a minimum at the cutoff frequency. In the presence of noise, the low signal-to-noise ratio (SNR) at high frequencies leads to a degraded resolution in practice. One straightforward strategy to mitigate the gain loss is to employ an annular pupil [15].

However, it leads to degraded optical sectioning and image artifacts. We aim here to present an alternative approach using a temporal modulation.

We previously demonstrated the use of spatiotemporal wavefront shaping for image reconstruction [16] in the acoustic regime. Using a rotating source as the illumination and a rotating receiver for the collection, we obtained different images corresponding to the convolutions of the object with different orthogonal PSFs. The PSFs present different topological phase structures. Owing to a periodic Doppler effect, a point-like object perceives a monochromatic wave field at ω_0 only on the rotation axis and a periodically modulated signal elsewhere with a frequency comb spectrum. For each harmonic frequency $\omega_0 + n\Omega$, the field forms a vortex with a vorticity n, centered on the optical axis. During the backscattering process, the same phenomenon applies, resulting in a focal spot twice as small as that of the full-field microscope at ω_0, and also vortex patterns twice as small as those in the focal plane at other frequencies. This suggests that the rotating emitter and recorder function acts as a spatiotemporal filter, retaining only the information associated with the high spatial frequency content collected by the confocal microscope. By exploiting the diversity of information by summing the images recovered from each PSF, an improvement of the confocal resolution by 70% is obtained demonstrating bandwidth extrapolation [17]. It enabled the discrimination of two point-like objects closer than $\frac{\lambda}{4NA}$, surpassing the confocal resolution.

This principle is broadly applicable to a wide range of wave-based imaging techniques [18]. We here apply it to an optical confocal scanning microscope. Similar concepts have been studied for the detection of rotating bodies in astronomy [19], and a closely related principle inspired by a synthetic aperture has been illustrated in a full-field configuration [20,21].

To engineer a high-speed, time-varying illumination with optical waves that will not significantly impede the confocal acquisition process, we opt to utilize a digital micromirror device (DMD) optically conjugated to the pupil plane of a microscope objective (Fig. 1(a)). This device enables amplitude modulation of the field at approximately 10 kHz. The time-varying pattern displayed modulates temporally the pupil function and, as a result, the CTF. Both the illumination and collection pupils are time-varying, which is equivalent to a rotation of the object via a change of frame. With this periodic acquisition scheme, n different images Im_n of the sample are collected (Fig. 1(b)). These images are convolutions of the object's reflectivity Obj and different PSFs such that

$$Im_n = Obj \otimes PSF_n, \tag{1}$$

with $\otimes$ being the spatial convolution operation.

In the following, we focus on a particular type of illumination consisting of a pattern rotating about the optical axis. We demonstrate how it enables the efficient extraction of the highest spatial frequency components allowing to improve the image resolution using a basic deconvolution scheme (Fig. 1(c)).

Numerical approach. We choose a sequence on the DMD, $M(x_d, y_d, t)$, consisting of the full pupil derived from a 45° truncated sector as depicted in Fig. 2(a).

Similar to a confocal microscope utilizing an annular aperture, we aim to ensure the optical sectioning capabilities of our approach while harnessing high spatial frequencies to guarantee optimal resolution [15]. Therefore, we have chosen a dynamic mask, the modulated part of which corresponds to a ring; the outer radius of this ring matches the maximum aperture of the optical system. We provide a mathematical description of these masks in Sect. 4.4 in Supplement 1. We have balanced the modulated and unmodulated portions of the mask to ensure a favorable SNR. The dynamic nature of the mask allows for the access of different spatial frequencies through various harmonics of the modulated signal, yielding an enhancement in contrast and resolution [16].

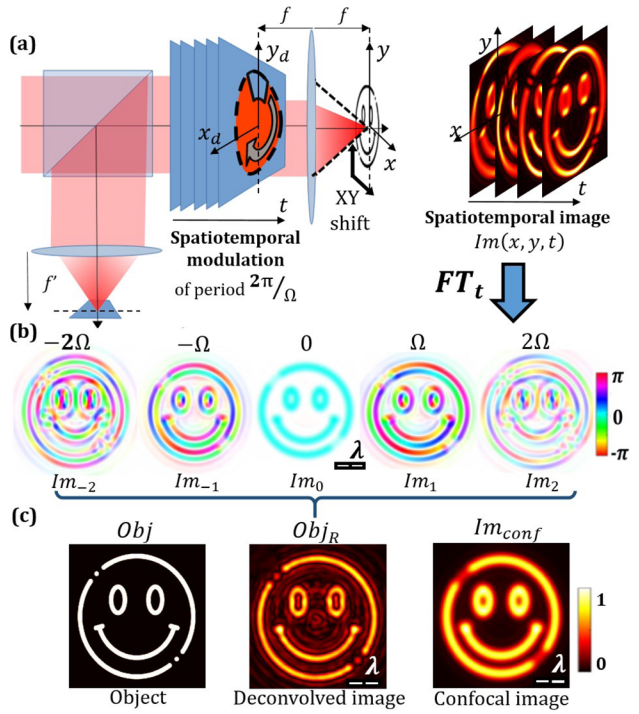

Fig. 1. Schematic view of the experimental process with simulated data. (a) Acquisition. A spatiotemporal image is acquired by scanning and temporally modulating the objective's pupil with a rotating mask in the Fourier plane of the object plane. (b) Analysis. Using a Fourier decomposition, we reconstructed complex images Im_n for harmonics associated with frequencies $n\Omega$ with $n \in \mathbb{Z}$. (c) Reconstruction. Each image Im_n is deconvolved using a computed PSF. A reconstruction of the sample Obj_R exhibiting sharper details than the confocal image Im_{conf} is obtained.

As a time-periodic pattern, it can be decomposed as a Fourier series with coefficients $M_n(x_d, y_d)$. As seen in Fig. 2(b), these coefficients are associated with vortices. Similarly, the corresponding temporal PSF or CTF can be computed and then again expressed as a Fourier series (Figs. 2(c) and 2(d)). As a topological invariant [22], the vorticity seen on the DMD patterns is conserved and is seen on the PSFs, thus guaranteeing their orthogonality. Indeed, the PSF corresponding to the frequency $n\Omega$ named PSF_n is a vortex of vorticity n with a radius increasing with $|n|$. It is associated with a coherent transfer function $CTF_n = \widehat{PSF_n}$ with $\widehat{.}$ being the Fourier transform operator. CTF_0 is roughly equivalent to the confocal CTF: the average pupil used during the illumination being almost the full microscope objective pupil, CTF_0 is also roughly the autoconvolution of the objective's pupil. The other dynamic CTFs possess a vorticity which imposes a zero for the low spatial frequencies (Fig. 2(d)). $CTF_{n\neq 0}$ carries information with a high gain only for the high spatial frequencies of the sample as with a thin annular aperture. This illustrates the benefit of using a rotating illumination

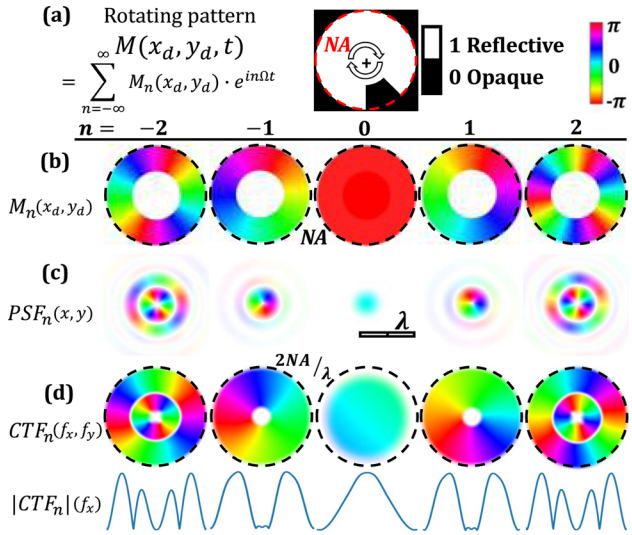

Fig. 2. PSF and CTF of the system associated with a given pattern decomposed as a Fourier series on the frequencies $n\Omega$ with $n \in [\![-2, 2]\!]$. (a) Rotating pattern M sent to the DMD. (b) Decomposition of $M(x_d, y_d, t)$. The pupil is a linear combination of vortex plates. (c) PSF in the sample's plane. (d) Coherent transfer functions (CTF_n) in the spatial frequency space (top) and modulus as a cross-sectional view (bottom). The dotted line represents the confocal resolution limit $2\lambda/NA$. The low spatial frequencies are not collected for values of n different than 0; CTF_0 corresponds roughly to the classical confocal CTF.

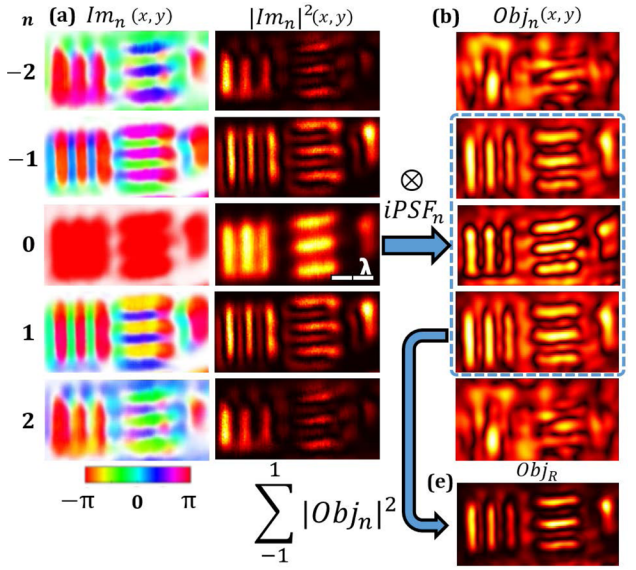

Fig. 3. Illustration of the deconvolution procedure with experimental images of a Ready Optics USAF resolution target group 11 element 1 (244 nm). (a) Dynamic confocal images obtained with the pattern of Fig. 2(a) at different harmonic frequencies $n\Omega$ for $n \in [\![-2; 2]\!]$ with weighted phase and intensity. (b) Deconvolved confocal dynamic images with numerical pseudoinverse $iPSF_n$. (c) Sum of Obj_n with $n \in [\![-1; 1]\!]$ to obtain a final reconstruction Obj_R.

in confocal microscopy since those frequencies are usually transmitted with a low gain leading to a resolution lower than $\frac{2NA}{\lambda}$ in the presence of noise.

The PSFs and CTFs can be computed analytically using a Fourier series decomposition and by applying the laws of Fourier optics (see Supplement 1). They match with the numerical simulation.

Experiment and results. The practical implementation of the experiment is represented in Fig. 1 and detailed in Supplement 1. It uses a narrowband polarized laser (Coherent Sapphire SF NX @488nm). The beam is enlarged, filtered, and modulated by a DMD and used to illuminate the sample, thanks to a microscope objective of numerical aperture $NA = 0.75$ (*Olympus* MPLFLN40X). The reflected light is sent to a *Thorlabs* PDA10A2 photodiode after being filtered by a pinhole whose equivalent size in the object plane is approximately 1 Airy unit. The current from the photodiode is amplified by a transimpedance amplifier and recorded by a *PicoScope* electronic oscilloscope. Using a 1951 *USAF* target, we estimate the white light full-field resolution to be 388 nm, for a theoretical value of $\lambda/2NA = 325$ nm. The confocal resolution is determined to be 244 nm in good agreement with $\frac{\lambda}{2\sqrt{2}NA} = 230$ nm (see Supplement 1).

For each position, the sequence of 60 masks $M(x_d, y_d, t)$ (illustrated in Fig. 2(a)) is displayed followed by a circular illumination associated with the full aperture. It allows the dynamic and *standard* confocal images to be acquired within the same sequence. After temporal Fourier decomposition of the received signals, we retrieve images at the different harmonics $n\Omega$ with $n \in [\![-2; 2]\!]$ (Fig. 3(a)). Each image provides a phase information that is reminiscent of the vortex nature of each PSF, carrying different information of the same object.

For $|n| > 1$, experimental data diverges from the theoretical and numerical predictions. A potential explanation is that higher-order vortices generated are not stable [23]. Other explanations involve the integrating effect with the finite size pinhole [14] and the setup's susceptibility to misalignment, thermal instability, and mechanical vibrations as reported in similar experiments [24].

To reconstruct the image associated with the nth harmonic, we implement a simple regularized inversion procedure. The image is deconvolved by its own inverted PSF predicted by the numerical simulation. To ensure the noise robustness of the inversion, a Tikhonov regularization is employed d [25,26]. The inverse operator writes

$$iCTF_n = \widehat{iPSF}_n = (CTF_n^* \cdot CTF_n + \sigma)^{-1} \cdot CTF_n^*, \qquad (2)$$

with σ the noise-to-signal ratio and $\cdot^*$ the complex conjugate. Note that the pseudo-inverse of a vortex-like PSF is also a vortex-like function with the opposite topological charge. Each image from each harmonic yields a reconstructed image referred to as Obj_n, given by $Obj_n = Im_n \otimes iPSF_n$. Results are shown in Fig. 3(b). Each image resembles the target object, albeit with noticeable degradation for $n = 2$, aligning with the discrepancies observed earlier. The final reconstruction Obj_R is achieved by summing all the deconvolved normalized intensity images so that $Obj_R = \sum Obj_n$, resulting in a pattern of enhanced contrast and improved resolution. Indeed, due to the orthogonality of the PSFs, each harmonic carries different information and noise contributions, leading to an improved SNR, particularly for high spatial frequencies.

We present in Fig. 4 the confocal images, both with and without inversion, alongside the results from our approach, pertaining to 218-nm-thick lines. The reconstructed image resulting from the temporally modulated wavefronts is the only one that

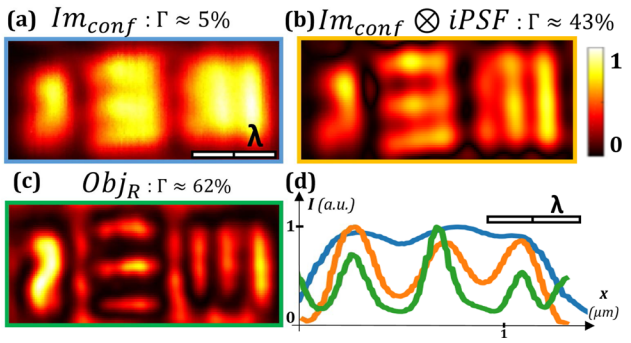

Fig. 4. Images at the resolution limit and associated contrast Γ. (a) Regular confocal image of group 11 element 2 of USAF target; the linewidth is 218 nm. (b) Deconvolution of the confocal image. (c) Reconstruction obtained by summing the deconvolved dynamic confocal images obtained with our method. This is a 10% improvement in resolution. (d) Cross-sectional view of the intensity profile for horizontal lines to highlight the improvement of the interline contrast $\Gamma = (I_{max} - I_{min})/(I_{max} + I_{min})$.

successfully allows discriminating the individual lines. This represents an approximately 10% improvement in resolution compared to the deconvolved confocal image with a better contrast (Fig. 4(d)).

Conclusion and perspectives. We propose incorporating temporal modulation into microscopy imaging techniques. As a demonstration, we apply rotating wavefronts in a confocal microscope. The introduction of a periodically rotating pattern results in the observation of harmonics, each allowing the reconstruction of a distinct image of the same sample. The vortex nature of the PSFs associated with these harmonics are used to selectively reconstruct information from different regions of the image's spatial spectrum. This leads to enhanced contrast and resolution. The reconstruction process is here limited to using only five harmonics. Imaging performance could be further improved by incorporating additional contributions, which requires precise estimation of higher-order PSFs. Additionally, integrating wavefront shaping hardware introduces technical complexities, as discussed in [23]. Addressing stability challenges and employing a more advanced reconstruction method should yield further enhancements.

The implementation of spatiotemporal modulation introduces new degrees of freedom, yet it still only requires a single photodetector for the measurement phase. This approach exemplifies PSF engineering, leveraging the spatiotemporal modulation of the illumination field to create controlled CTFs for different harmonics. This concept is adaptable to various optical setups in a full-field configuration, such as in image scanning microscopy [27] or with photodiode arrays for pixel reassignment [28], but also in astronomy, for instance, using coronagraphy [29].

Funding. Agence Nationale de la Recherche (Labex WIFI); Simons Foundation (Symmetry-Driven Extreme Wave Phenomena).

Disclosures. The authors declare no conflicts of interest.

Data availability. Data and codes underlying the results presented here may be obtained from the authors upon reasonable request.

Supplemental document. See Supplement 1 for supporting content.

REFERENCES

1. M. Minsky, "Microscopy apparatus", U.S. patent 3,013,467 (1957).
2. T. R. Corle and G. Kino, *Confocal Scanning Optical Microscopy and Related Imaging Systems* (Academic Press, 1996).
3. J. Jonkman, C. M. Brown, G. D. Wright, *et al.*, Nat. Protoc. **15**, 1585 (2020).
4. T. Klar, E. Engel, and S. Hell, Phys. Rev. E **64**, 066613 (2001).
5. V. Marx, Nat. Methods **16**, 1209 (2019).
6. V. Astratov, *Label-Free Super-Resolution Microscopy* (Springer, 2019).
7. N. Engheta, Science **379**, 1190 (2023).
8. M. Rust, M. Bates, and X. Zhuang, Nat. Methods **3**, 793 (2006).
9. M. G. L. Gustafsson, J. Microsc. **198**, 82 (2000).
10. T. Dertinger, R. Colyer, G. Iyer, *et al.*, Proc. Natl. Acad. Sci. U. S. A. **106**, 22287 (2009).
11. P. Jouchet, C. Cabriel, N. Bourg, *et al.*, Nat. Photonics **15**, 297 (2021).
12. A. W. Lohmann, R. G. Dorsch, D. Mendlovic, *et al.*, J. Opt. Soc. Am. A **13**, 470 (1996).
13. J. Mertz, *Introduction to Optical Microscopy*, 2nd ed. (Cambridge University Press, 2019).
14. T. Wilson and C. Sheppard, *Theory and Practice of Scanning Confocal Microscopy* (Academic Press, 1984).
15. C. J. R. Sheppard and T. Wilson, Appl. Opt. **18**, 3764 (1979).
16. G. Noetinger, S. Métais, G. Lerosey, *et al.*, Phys. Rev. Appl. **19**, 024032 (2023).
17. J. W.Goodman, *Introduction to Fourier Optics*, 3rd ed. (Roberts & Company, 2005).
18. R. D. Weglein and R. G. Wilson, Appl. Phys. Lett. **31**, 793 (1977).
19. M. P. J. Lavery, F. C. Speirits, S. M. Barnett, *et al.*, Science **341**, 537 (2013).
20. D. Ruh, J. Mutschler, M. Michelbach, *et al.*, Optica **5**, 1371 (2018).
21. Y. Cotte, F. Toy, J. Pascal, *et al.*, Nat. Photonics **7**, 113 (2013).
22. G. Indebetouw, J. Mod. Opt. **40**, 73 (1993).
23. V. Berry and R. M. Dennis, J. Opt. **19**, 1 (2017).
24. A. A. Pushkina, G. Maltese, J. I. Costa-Filho, *et al.*, Phys. Rev. Lett. **127**, 253602 (2021).
25. A. Tikhonov, Soviet Math. Dokl. **4**, 1035 (1963).
26. S. Popoff, G. Lerosey, M. Fink, *et al.*, Nat. Commun. **1**, 81 (2010).
27. C. B. Müller and J. Enderlein, Phys. Rev. Lett. **104**, 198101 (2010).
28. T. B. DuBose, F. LaRocca, S. Farsiu, *et al.*, Nat. Photonics **13**, 257 (2019).
29. A. Aleksanyan, N. Kravets, and E. Brasselet, Phys. Rev. Lett. **118**, 203902 (2017).